



RESEARCH

Open Access



Enhanced delivery of a low dose of aducanumab via FUS in 5 × FAD mice, an AD model

Chanho Kong^{1†}, Eun-Jeong Yang^{2,3†}, Jaewoo Shin^{1†}, Junwon Park¹, Si-Hyun Kim^{2,3}, Seong-Wook Park², Won Seok Chang¹, Chang-Han Lee^{2,4}, Hyunju Kim^{2,3*}, Hye-Sun Kim^{4,5*}  and Jin Woo Chang^{1*} 

Abstract

Background: Aducanumab (Adu), which is a human IgG1 monoclonal antibody that targets oligomer and fibril forms of beta-amyloid, has been reported to reduce amyloid pathology and improve impaired cognition after administration of a high dose (10 mg/kg) of the drug in Alzheimer's disease (AD) clinical trials. The purpose of this study was to investigate the effects of a lower dose of Adu (3 mg/kg) with enhanced delivery via focused ultrasound (FUS) in an AD mouse model.

Methods: The FUS with microbubbles opened the blood–brain barrier (BBB) of the hippocampus for the delivery of Adu. The combined therapy of FUS and Adu was performed three times in total and each treatment was performed biweekly. Y-maze test, Brdu labeling, and immunohistochemical experimental methods were employed in this study. In addition, RNA sequencing and ingenuity pathway analysis were employed to investigate gene expression profiles in the hippocampi of experimental animals.

Results: The FUS-mediated BBB opening markedly increased the delivery of Adu into the brain by approximately 8.1 times in the brains. The combined treatment induced significantly less cognitive decline and decreased the level of amyloid plaques in the hippocampi of the 5 × FAD mice compared with Adu or FUS alone. Combined treatment with FUS and Adu activated phagocytic microglia and increased the number of astrocytes associated with amyloid plaques in the hippocampi of 5 × FAD mice. Furthermore, RNA sequencing identified that 4 enriched canonical pathways including phagosome formation, neuroinflammation signaling, CREB signaling and reelin signaling were altered in the hippocampi of 5 × FAD mice receiving the combined treatment.

Conclusion: In conclusion, the enhanced delivery of a low dose of Adu (3 mg/kg) via FUS decreases amyloid deposits and attenuates cognitive function deficits. FUS-mediated BBB opening increases adult hippocampal neurogenesis

[†]Chanho Kong, Eun Jeong Yang, Jaewoo Shin: These authors contributed equally to this work

*Correspondence: hj-k89@hanmail.net; hyisun@snu.ac.kr; jchang@yuhs.ac

¹ Department of Neurosurgery, Yonsei University College of Medicine, 50 Yonsei-Ro, Seodaemun-Gu, Seoul, Republic of Korea

² Department of Pharmacology, College of Medicine, Seoul National University, 103 Daehakro, Jongro-Gu, Seoul, Republic of Korea

⁴ Department of Biomedical Sciences, College of Medicine, Seoul National University, 103 Daehakro, Jongro-Gu, Seoul, Republic of Korea
Full list of author information is available at the end of the article



as well as drug delivery. We present an AD treatment strategy through the synergistic effect of the combined therapy of FUS and Adu.

Keywords: Aducanumab, Alzheimer's disease, Focused ultrasound, Transcriptome profiling

Introduction

Alzheimer's disease (AD) is the most common neurodegenerative disease where cognitive functions, including memory, progressively deteriorate. Pathological features of AD include extracellular beta-amyloid (A β) plaques and intracellular neurofibrillary tangles, leading to neurodegeneration and neuronal cell death. There have long been only four FDA-approved treatments for AD, including donepezil, rivastigmine, and galantamine, which alleviate symptoms by inhibiting acetylcholinesterase activity, and memantine which is a partial NMDA antagonist [1]. According to the recently reported AD drug development pipeline and especially after the United States Food & Drug Administration (FDA) approved aducanumab (Adu), the recent treatment development tends to be progressing more toward the fundamental treatment of the disease rather than merely focusing on symptom relief [2, 3].

Adu, a human IgG1 antibody designed for targeting aggregated oligomer and fibril forms of A β , was approved by the FDA in 2021 [4] and is the first disease-modifying drug being used to slow the progression of AD and treat patients with mild cognitive impairment or the mild dementia stage of disease [5]. In a clinical study, the accumulation of A β in the hippocampus was decreased by Adu in a dose-dependent manner (3–10 mg/kg) [1]. Consistent with the aforementioned outcome of a clinical trial, an animal study using an AD mouse model (Tg2576) showed that A β was significantly reduced in the group given a dose of 10 mg/kg or higher (30 mg/kg) [5]. Acting as a double-edged sword, the blood-brain barrier (BBB) is essential for maintaining brain homeostasis. However, its function has long been a challenge in regard to applying potentially effective therapeutic agents, as BBB prevents approximately 98% of drug compounds with high molecular weight such as antibodies from penetrating the parenchyma [6]. Concentrating the acoustic pressure on the target area in the brain causes the cavitation effect of circulating microbubbles and temporarily opens the BBB [7]. Focused ultrasound (FUS) with microbubbles causes reversible opening of the BBB to both small and large molecules [8]. There are studies on the delivery of various therapeutic agents, such as chemotherapeutics [9–11] and cells [12–14]. Furthermore, multiple pieces of evidence have reported that cerebral A β levels and plaque burden are reduced by opening the BBB only without delivering therapeutic agents in AD mouse

models [15–17]. Previously, we and other research groups reported that BBB opening by FUS increased adult hippocampal neurogenesis in rodents, which implies that FUS has therapeutic potential as an effective therapeutic strategy for AD [18–20].

Even though Adu has been approved by the FDA via an accelerated approval program, there may still be a challenging task in clinical phase IV. A previous study reported that only approximately 1.3% of Adu can reach the brain due to its large size by systemic administration. In addition, a high concentration (10–60 mg/kg) of Adu could not be used because of its side effects such as amyloid-related imaging abnormalities including edema (ARIA-E) or microhemorrhage/superficial siderosis (ARIA-H) [5]. In this study, we investigated the effects of a lower dose of Adu (3 mg/kg) with FUS in an AD mouse model.

Methods

Animals

The 5 familial AD mutations (5 \times FAD) mouse is a transgenic mouse with five familial mutations observed from early-onset AD families. This mouse expresses high levels of both mutant human amyloid precursor protein (APP695) with Swedish mutation (K670N, M671L), London mutation (V717I), Florida mutation (I716V), and human presenilin 1 (PS1) with two mutations (M146L and L286V). 5 \times FAD mice were purchased from Jackson Laboratory (Sacramento, CA) and maintained by crossing hemizygous transgenic mice with B6SJL F1 mice. The transgenic mice were identified by polymerase chain reaction, and non-transgenic littermates served as wild type (WT). The main characteristics of 5 \times FAD mice are extracellular amyloid deposition and gliosis beginning around 2 months [21]. Also, its phenotype can be defined as spontaneous alternation in the Y maze in that the impairment in spatial working memory begins at approximately 4–5 months of age [21, 22]. Neuron loss has been observed in multiple brain regions in this model and begins at about 6 months of age [21, 23]. All mice were housed in groups of 2–5 per cage with ad libitum access to food and water, in a humidity- and temperature-controlled, specific pathogen-free environment (12 h light cycle; lights on at 8 AM) in the Institute for Experimental Animals of Seoul National University. All experiments were approved by the Animal Care

Committee of Seoul National University (Approval Number: SNU-201005-2-1).

Focused ultrasound

A 0.5 MHz single element focused transducer (H-107MR; SonicConcepts, Bothell, WA) was used. The diameter of the transducer was 51.7 mm and the radius of curvature was 63.2 mm. The transducer was used with a conical container that could be filled with degassed water to efficiently transfer acoustic energy. A waveform generator (33220A, Agilent, Palo Alto, CA) was connected to a 40 dB Radio Frequency Power Amplifier (210 L, ENI Inc., Rochester, NY) to drive the FUS transducer, and a power meter (E4419B, Agilent) was used to measure the input electrical power (Fig. 1a).

Magnetic resonance imaging (MRI)

MRI was performed immediately following sonication with a Bruker 9.4 T 20 cm bore MRI system (Biospec 94/20 USR; Bruker, Ettlingen, Germany) and mouse head coil. A gadolinium-based MRI contrast agent, Gadobutrol (Gd; Gadovist; 0.2 ml/kg), was injected

Table 1 MRI sequences and parameters

	T1-weighted imaging
Echo	1
TR (ms)	500
TE (ms)	8.1
FA (deg)	90
NEX	5
FOV (cm)	2 × 2
Matrix	256 × 256

intravenously. MRI sequence parameters are summarized in Table 1.

Preparation of Adu

VH and VL sequences were identified in Biogen Idec’s patent submission for WO2014089500A1 and were cloned into human IgG2a and kappa pcDNA3.1 vectors (GenScript, NJ). Human Adu was produced using the Expi293 expression system and purified using protein A/G microbeads (Thermo Fisher Scientific, MA).

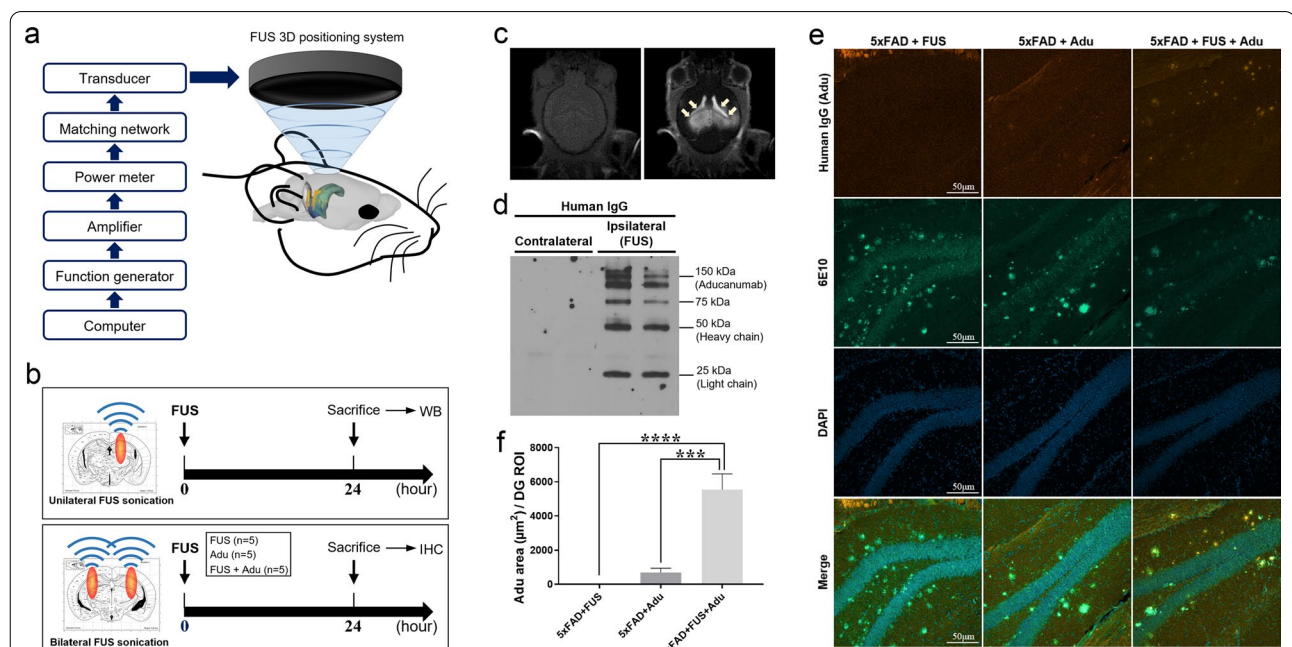


Fig. 1 FUS-mediated BBB opening significantly increased the delivery of Adu in the brain. **a** A scheme of the FUS system set up for BBB opening in mice. **b** A schematic diagram for unilateral (upper panel) and bilateral (lower panel) FUS sonication. **c** Pre- and post-gadolinium T1-weighted images: FUS-mediated BBB opening was confirmed with MRI. **d** FUS was treated unilaterally to the brains of experimental animals. A representative image of Western blotting with an antibody against human IgG after Adu injection and unilateral FUS treatment. **e** Representative confocal images (20x) of human IgG (Aducanumab), Aβ stained with 6E10 antibody and DAPI in the dentate gyrus of the hippocampus. **f** A bar graph showing the levels of Adu assessed with human IgG antibody in the hippocampus. Data are presented as mean ± SEM. Statistical analyses were performed using one-way ANOVA, followed by Tukey’s post hoc analysis. (*****P* < 0.0001, ****P* < 0.001, *n* = 5 mice for each group)

Preparation of aggregated A β peptide

Aggregated A β was prepared according to a previous study [24]. Briefly, 1 mg of lyophilized A β (Anaspec, AS-20276, CA, USA) was dissolved in hexafluoroisopropanol (HFIP) (Sigma-Aldrich, 105228, MO). The A β -HFIP solution (1 mM) was incubated at room temperature for 30 min. Then, A β was lyophilized by evaporating HFIP in a fume hood overnight. To remove remaining HFIP and moisture, A β was transferred to a HyperVAC-LITE (Hanil, HVC-2124, Gyeonggido, Korea) and dried for 1 h.

Enzyme-linked immunosorbent assay (ELISA)

To determine the concentration of Adu in the serum, 16.13 ng of aggregated A β per well was coated to 96-well ELISA plates (Thermo Fisher Scientific, #439,454) overnight at 4 °C. Then, the plates were blocked with phosphate-buffered saline (PBS) supplemented with 3% BSA for 2 h at room temperature. Next, 50-fold diluted serum in PBS was added and incubated for 1 h at room temperature. After washing with PBS with 0.05% (*v/v*) tween20 (PBS-T), the bound serum antibodies were detected by an HRP-conjugated rabbit anti-human IgG (Invitrogen, #A18903, 1:500, MA). After washing with PBS-T four times, 50 μ l of 3,3',5,5'-tetramethylbenzidine (Thermo Fisher Scientific, #34028) was added per well as a chromogen substrate. The plate was kept at room temperature for 2 min 30 s, and the reaction was terminated by adding 50 μ l of 2 M H₂SO₄. Absorbance at 450 nm was measured on an infinite M200 PRO (TECAN). The results are presented after subtracting the control value from 5 \times FAD-Sham mouse serum value. For the standard curve of Adu in the serum, 5 \times FAD-Sham mouse serum was used. Serially diluted Adu (100 nM, 50 nM, 25 nM, 12.5 nM, 6.25 nM, 3.125 nM) was added in 50-fold diluted 5 \times FAD-Sham mouse serum, and the concentrations were determined using the same method as above.

Confirmation of Adu delivery by FUS-mediated BBB opening

A schematic diagram for unilateral or bilateral FUS sonication is shown in Fig. 1b. First, FUS was unilaterally sonicated into the hippocampus of the 5 \times FAD mice to confirm whether Adu was delivered into the brains of 5 \times FAD mice by FUS-mediated BBB opening. Then, 24 h later, the mice were sacrificed and the contralateral hemispheres were compared. Second, we quantified Adu to determine whether the combined treatment with FUS enhanced the delivery of Adu into the brain. The 5 \times FAD mice were divided into three groups: the 5 \times FAD + FUS, 5 \times FAD + Adu, and 5 \times FAD + FUS + Adu. The FUS was sonicated to the hippocampus bilaterally. Adu was

injected intravenously immediately after FUS sonication, and the mice were sacrificed 24 h later.

Combined treatment with FUS and Adu

All mice were divided into five groups: WT-Sham, 5 \times FAD-Sham, 5 \times FAD + Adu, 5 \times FAD + FUS and 5 \times FAD + FUS + Adu groups. For treatment, mice were anesthetized with 5% isoflurane in oxygen and animal heads were fixed on a stereotaxic frame (Narishige, Tokyo, Japan). Medical sterile ultrasound gel (ProGel-Dayo Medical Co, Seoul, South Korea) was used to fill the space between a coupling cone full of degassed water and the skull for energy transfer efficiency. The FUS was bilaterally targeted to four focal spots in the hippocampus. DEFINITY microbubbles (0.04 ml/kg; Lantheus Medical Imaging, North Billerica, MA) were injected intravenously 10 s before sonication. FUS (1-Hz burst repetition frequency, 10-ms bursts, 120 s in total, and average peak pressure 0.25 MPa) was started at the same time (Fig. 1a). Adu (3 mg/kg in saline) was injected intravenously at the end of FUS sonication. It was delivered three times in total and each treatment was performed every two weeks (Fig. 2a).

Western blotting

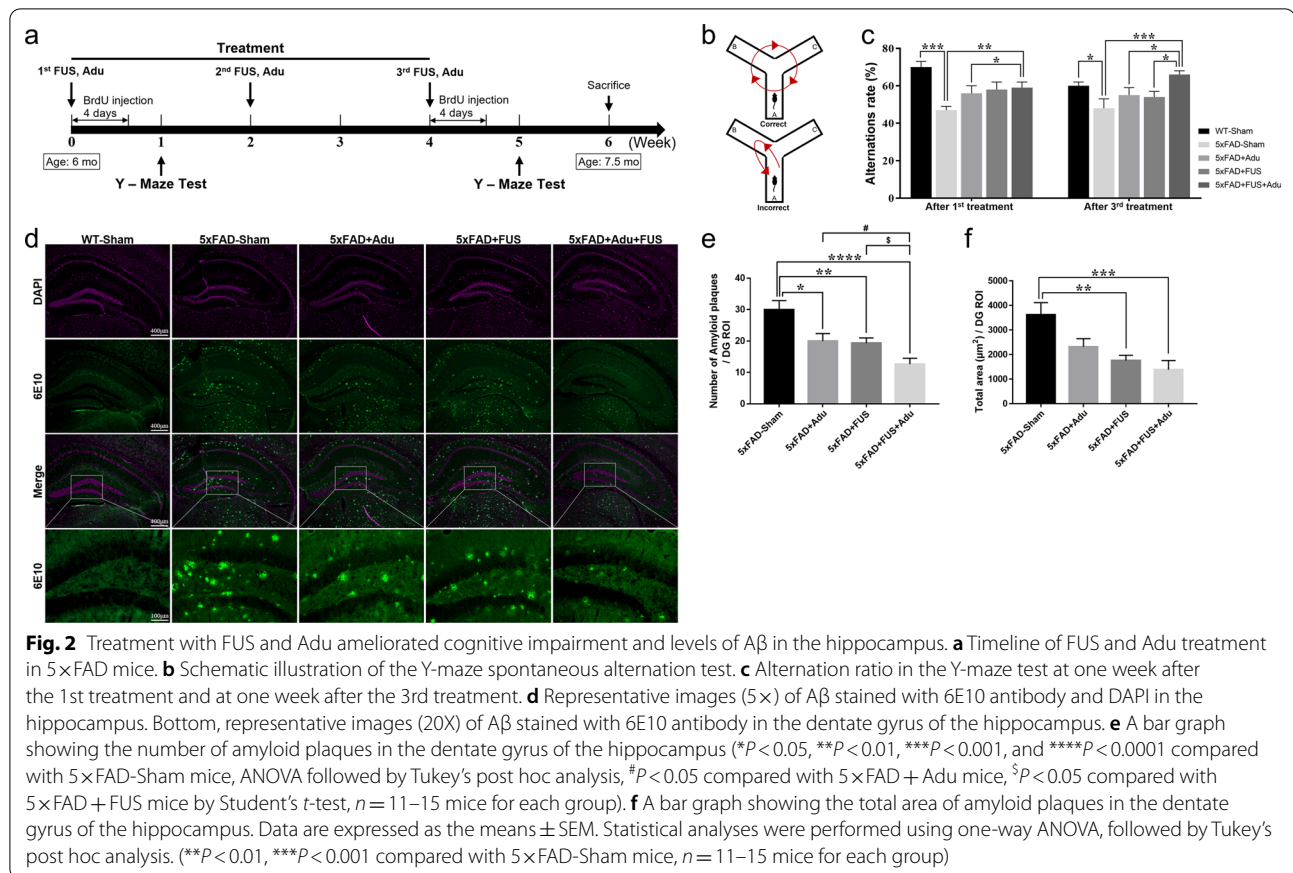
Hippocampal lysates were resolved on a 10% SDS-PAGE gel and transferred to the nitrocellulose membrane, followed by blocking with 5% skim milk. The antibody used was anti-human IgG-HRP (Invitrogen, A18903, 1:2000, CA). The relative intensity of blots was quantified using ImageJ software.

Spontaneous alternation Y-maze test

To investigate spatial working memory, spontaneous alternation in the Y-maze was investigated in experimental animals (Fig. 2b). Y-maze test was performed three times 1 week after each treatment (Fig. 2a). The alternation performance was tested using asymmetrical Y-maze, consisting of 3 equal arms (40 \times 15 \times 9 cm³), and constructed using black acrylic plastic. All mice were placed at the center of the Y-maze and allowed to explore freely for 8 min. All movements were recorded using a video camera and were analyzed to determine the alternation ratio by manually evaluating the number of triads containing entries into all three arms.

5-Bromo-2'-deoxyuridine (BrdU) labeling

BrdU was injected intraperitoneally twice a day for 4 days after treatment. To investigate the acute and chronic effects of treatment on cell proliferation, neuronal



differentiation and cell survival in the hippocampus, we divided cells into two different time points of BrdU injection after the 1st and 3rd treatments. (Fig. 2a).

Immunohistochemistry

Brains were fixed with 4% paraformaldehyde for 24 h, transferred to 30% sucrose for 3 days and stored at -20°C in cryoprotectant storage solution until use. Brains were cut into 30- μm coronal sections. Free-floating sections were washed in PBS and incubated in blocking solution (PBS, 5% normal goat serum, 0.2% Triton X-100) for 3 h at room temperature. Sections were incubated with primary antibodies in blocking solution overnight at 4°C . The primary antibodies used were as follows: ZO-1 (Invitrogen, 61-7300, 1:1000, CA), BrdU (Abcam, ab6326, 1:250, Cambridge, UK), NeuN (Millipore, ABN78, 1:500, MA, USA), 6E10 (anti-A β aa 1–16 antibody, Biogen, SIG39320, 1:500, CA), Iba-1 (Novus Biologicals, NB100-1028, 1:150, CO, USA or Wako, 19-19741, 1:150, VA), CD68 (Bio-Rad, MCA1957, 1:150, CA), and GFAP (Abcam, ab53554, 1:150, MA). After the primary immunoreaction, sections were incubated with Alexa 488 (Invitrogen, A11008, 1:500, CA) or Alexa 594 (Abcam, A150156, 1:250, MA) conjugated secondary

antibodies. For detection of Adu penetration into the brain, brain sections were incubated with anti-human IgG Alexa 555 (Invitrogen, A21433, 1:200, CA). Immunostaining of the sections was visualized with an LSM 700 confocal microscope (Carl Zeiss, Jena, Germany) or an Axio Imager M2 (Carl Zeiss) light microscope. Images were analyzed using ImageJ software (Version 1.52a, NIH, USA).

Quantification of A β plaque-associated microglia and astrocytes

The quantification of A β plaque-associated microglia and astrocytes was performed using a previously reported method with minor modification [25]. Z-stacks (30 μm) were collected with 1 μm between each slice. Within 20 μm from the A β plaques, the number of Iba-1 or GFAP-positive cells was manually counted. Only those microglia or astrocytes whose nuclei were present in the Z-stack were included in the analysis. The size of the A β deposits was calculated from maximum projections of 6E10 immunoreactivity and subsequently used to determine the number of microglia or astrocytes surrounding the A β deposits of different sizes.

RNA sequencing and ingenuity pathway analysis (IPA)

Three to four hippocampal samples per group were randomly selected for RNA sequencing analysis. Total RNA was extracted using a QIAGEN miRNeasy mini kit (Qia-gen #217004). RNA (116 ng) was used to prepare RNA sequencing libraries using Illumina Stranded Total RNA Prep Ligation with Ribo-Zero Plus. The libraries were sequenced by an Illumina HiSeq 3000 sequencer at Yonsei Genome Center (Seoul, South Korea). The data preprocessing included a quality check by FastQC and, where needed, trimming of the adapter sequences by Trimmomatic v0.32. The raw reads were aligned to the mouse reference genome (mm10) using the HISAT2 splice-aware aligner. The transcripts per million were quantified using StringTie. Significantly differentially expressed genes (DEGs) were defined by adjusted *P* values (*q* values) less than 0.05. For the canonical pathway, upstream regulatory networks, and molecular networks of DEGs, we used the commercial QIAGEN Ingenuity® Pathway Analysis (IPA®, QIAGEN Redwood City, www.qiagen.com/ingenuity) software. For the canonical pathway analysis, $-\log(q \text{ value}) > 1.3$ was taken as the threshold, a Z score > 1 was defined as the threshold of activation, and a Z score < -1 was defined as the threshold of inhibition. For upstream regulators, $-\log(q \text{ value}) > 1.3$ was set as the threshold. The score was calculated by IPA for molecular networks, and significant changes in DEGs in the WT-Sham/5×FAD-Sham/5×FAD + FUS + Adu dataset were used for the comparison analysis.

Statistical analysis

All data are expressed as the mean \pm standard error of the mean. Data were calculated using a one-way analysis of variance (ANOVA) and Kruskal–Wallis test followed by a least significant different (LSD) and Tukey's post hoc analysis. In addition, Student's *t*-test was also used. A value of $P < 0.05$ was considered statistically significant for all measures. All statistical analyses were performed using SPSS (Version 25, SPSS Inc., Chicago, IL) and GraphPad Prism 8 software (GraphPad Software Inc., San Diego, CA).

Results

FUS markedly improved the delivery of Adu into the targeted region of the brain, and Adu specifically bound to amyloid plaques in the hippocampi of 6–7 month-old 5×FAD mice

First, we confirmed the safety of FUS sonication in experimental animals. Previously, several groups, including our own, have demonstrated the safety of FUS [26, 27]. Here, we investigated the expression level of ZO-1 (Zonula occludens-1), which is a tight junction-associated protein reflecting the intactness of BBB, to confirm the safety

of FUS in our model. The protein level of ZO-1 did not significantly differ among the WT-Sham, 5×FAD-Sham, 5×FAD + Adu, 5×FAD + FUS and 5×FAD + FUS + Adu groups 24 h after FUS sonication (Additional file 1: Fig. S1), indicating that there was no significant difference between the WT and 5×FAD or FUS sonication groups. Then, we investigated whether FUS with microbubbles can specifically open the BBB in targeted brain regions. After FUS sonication, we first acquired MR images without gadolinium and then performed MRI again with gadolinium to confirm whether the BBB is properly open. As shown in Fig. 1c, BBB opening in the hippocampus was confirmed through contrast-enhanced MRI. Then, to measure the increased delivery of Adu into the hippocampus after BBB opening by FUS treatment, we analyzed the hippocampal regions. FUS was given unilaterally (only to one hemisphere) to the hippocampus of experimental animals (Fig. 1b). A larger amount of intravenously administered Adu was detected in the ipsilateral region but not in the contralateral region (Fig. 1d).

We also quantified the amount of Adu in the brains 24 h after the treatment to investigate whether the combined treatment with bilateral FUS enhanced the delivery of Adu into the brains by immunohistochemistry. The FUS + Adu group markedly increased the delivery of Adu at 24 h compared with the Adu only group by approximately 8.1 times (Adu: 683 ± 259 /dentate gyrus region of interest (ROI), FUS + Adu; $5541 \pm 92 \mu\text{m}^2$ /dentate gyrus ROI) (Fig. 1e and f). To confirm the specific binding of Adu with amyloid deposits in the hippocampus, costaining with 6E10 and Adu antibodies was assessed. The colocalization of amyloid plaques with Adu was observed in the combined treatment group (Fig. 1e).

In addition, dose-dependent brain delivery of Adu by FUS was examined 24 h after FUS sonication in 6-month-old 5×FAD mice by performing Western blotting. A dose-dependent increase in the amount of Adu of the brain, as assessed with human IgG, was observed. In both the 3 and 10 mg/kg Adu without FUS groups, very little Adu was detected by Western blotting (Additional file 1: Fig. S2). Based on these results, the delivery of Adu (3 and 10 mg/kg) with FUS was significantly higher than the delivery of Adu without FUS, supporting our hypothesis that a lower dose of Adu (3 mg/kg) can exert therapeutic effects when applied with FUS sonication. The serum concentration of Adu was also investigated by ELISA assay with aggregated A β peptides at 1 and 24 h after intravenous injection with or without FUS sonication in 6-month-old 5×FAD mice. As expected, the 5×FAD + FUS + Adu group showed a significantly lower serum Adu concentration than the 5×FAD + Adu group. At a low dose (3 mg/kg), the 5×FAD + FUS + Adu group showed an approximately 33.5% lower Adu

concentration than the 5×FAD + Adu after 1 h, and the 5×FAD + FUS + Adu group showed an approximately 50.5% lower Adu concentration than the 5×FAD + Adu after 24 h. Similarly, at a high dose (10 mg/kg), the 5×FAD + FUS + Adu group showed an approximately 12.9% lower Adu concentration than the 5×FAD + Adu after 1 h, and the 5×FAD + FUS + Adu group showed an approximately 38.8% lower Adu concentration than the 5×FAD + Adu after 24 h (Additional file 1: Fig. S3). These results are correlated with the brain results.

Combined treatment with FUS and low dose of Adu (3 mg/kg) ameliorated cognitive impairments and significantly reduced the levels of amyloid plaques in the dentate gyrus of the hippocampus of 6 to 7-month-old 5×FAD mice

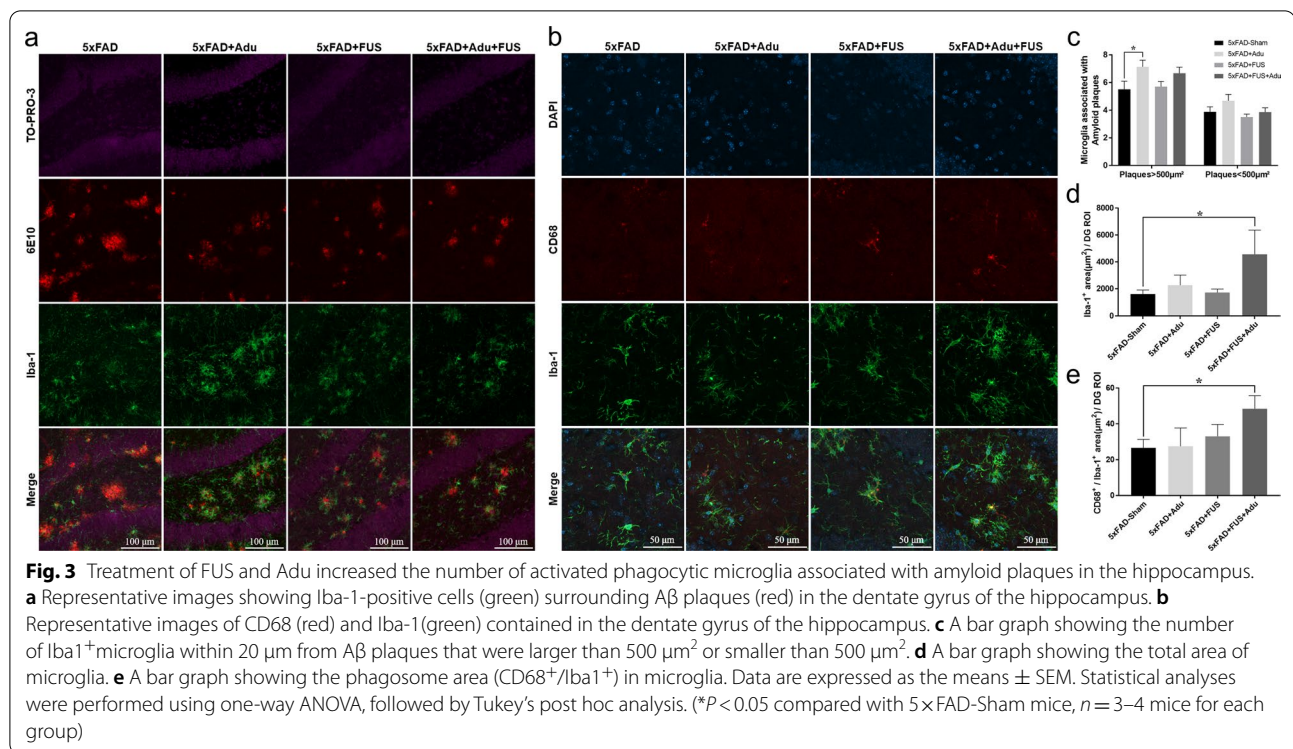
To investigate the effect of combined treatment with FUS and Adu on cognitive impairment in 5×FAD mice, spatial learning memory was assessed using the Y-maze test. After the 1st treatment, the combined treatment group with FUS and Adu featured a significantly increased alternation ratio compared with 5×FAD-Sham mice and 5×FAD + Adu mice (Fig. 2c, WT-Sham: 69.7 ± 2.5%, 5×FAD-Sham: 46.7 ± 2.1%, 5×FAD + Adu: 55.9 ± 3.6%, 5×FAD + FUS: 58.1 ± 4.1%, 5×FAD + FUS + Adu: 59.1 ± 2.6%). After the 3rd treatment, the combined treatment group exhibited a higher alternation ratio than the 5×FAD-Sham mice, the 5×FAD + Adu mice, and the 5×FAD + FUS mice (Fig. 2c, WT-Sham: 60.6 ± 2.1%, 5×FAD-Sham: 47.8 ± 4.5%, 5×FAD + Adu: 54.6 ± 3.6%, 5×FAD + FUS: 53.8 ± 3.8%, 5×FAD + FUS + Adu: 65.8 ± 2.0%). The combined treatment with FUS and Adu was significantly effective in alleviating the cognitive dysfunction assessed with the Y-maze test than the treatment with Adu or FUS alone. The combined treatment with FUS and Adu contributed to significantly improved cognitive impairment in the 5×FAD mice. To measure the therapeutic effects of combined treatment with FUS and Adu, we analyzed the accumulation of amyloid plaques in the hippocampus through immunostaining with 6E10 antibody. In the brains of WT-Sham mice, amyloid plaques were not observed at this age (7.5 months old, Fig. 2d).

All groups showed a significantly reduced number of amyloid plaques in the dentate gyrus of the hippocampus compared with 5×FAD-Sham; in particular, the decrease was remarkably reduced in the 5×FAD + FUS + Adu group (Fig. 2e, 5×FAD-Sham: 29.9 ± 2.9, 5×FAD + Adu: 20.0 ± 2.3, 5×FAD + FUS: 19.3 ± 1.6 and 5×FAD + FUS + Adu: 12.6 ± 1.9/dentate gyrus ROI). Additionally, areas of decreased Aβ were measured and compared. 5×FAD + FUS and 5×FAD + FUS + Adu groups showed a significantly reduced total area of amyloid plaques in the dentate

gyrus of the hippocampus compared with 5×FAD-Sham group (Fig. 2f, 5×FAD-Sham: 3614 ± 498, 5×FAD + Adu: 2316 ± 331, 5×FAD + FUS: 1755 ± 218, 5×FAD + FUS + Adu: 1385 ± 374.3/dentate gyrus ROI). Thus, repeated combined treatment with FUS and Adu contributed to significantly improved cognitive impairment in the 5×FAD mice. Taken together, the combined treatment of Adu with FUS significantly ameliorated the amyloid plaque load in the hippocampi of 5×FAD mice compared with Adu or FUS alone.

Combined treatment with FUS and Adu induced activation of phagocytic microglia and increased astrocytes associated with amyloid plaques in the hippocampi of 5×FAD mice

Microglia and astrocytes clear pathological deposits of molecules such as Aβ through phagocytosis and degradation in the central nervous system (CNS) [28]. To measure the localization of amyloid plaque-associated microglia, immunostaining of Iba-1, which is well known as a marker of microglia, was performed for the four experimental groups, including 5×FAD-Sham, 5×FAD + Adu, 5×FAD + FUS, and 5×FAD + FUS + Adu (Fig. 3a). The number of reactive microglia within 20 μm from amyloid plaques larger than 500 μm² was significantly increased only in the 5×FAD + Adu group compared with the 5×FAD-Sham group (Fig. 3c, 5×FAD-Sham: 5.5 ± 0.60, 5×FAD + Adu: 6.8 ± 0.4, 5×FAD + FUS: 5.7 ± 0.3, 5×FAD + FUS + Adu: 6.6 ± 0.4/amyloid plaque). These data indicate that Adu treatment alone recruited microglia to large amyloid plaques. No significant difference was observed in the number of microglia within 20 μm from amyloid plaques smaller than 500 μm² in all groups (Fig. 3c, 5×FAD-Sham: 3.8 ± 0.3, 5×FAD + Adu: 4.6 ± 0.47, 5×FAD + FUS: 3.5 ± 0.2 and 5×FAD + FUS + Adu: 3.8 ± 0.3/amyloid plaque). Then, we examined the Iba-1⁺ microglial area and Iba-1⁺/CD68⁺ microglia to investigate whether the activation of microglia and potential phagocytic activity in microglia were altered in all groups. CD68, a marker associated with phagocytic activity, is increased in the AD brain [29]. The Iba-1⁺ area in the dentate gyrus of the hippocampus was increased in the combined treatment group compared with the 5×FAD-Sham group (Fig. 3b, d, and e; 5×FAD-Sham: 1600 ± 304 μm², 5×FAD + Adu: 2264 ± 760 μm², 5×FAD + FUS: 1716 ± 257 μm² and 5×FAD + FUS + Adu: 4568 ± 1976 μm²/dentate gyrus ROI). The co-stained area with Iba-1 and CD68, which is a lysosome-associated membrane protein involved in phagocytosis and is used as a marker for macrophages and other mononuclear phagocytes, in the dentate gyrus of the hippocampus was significantly increased



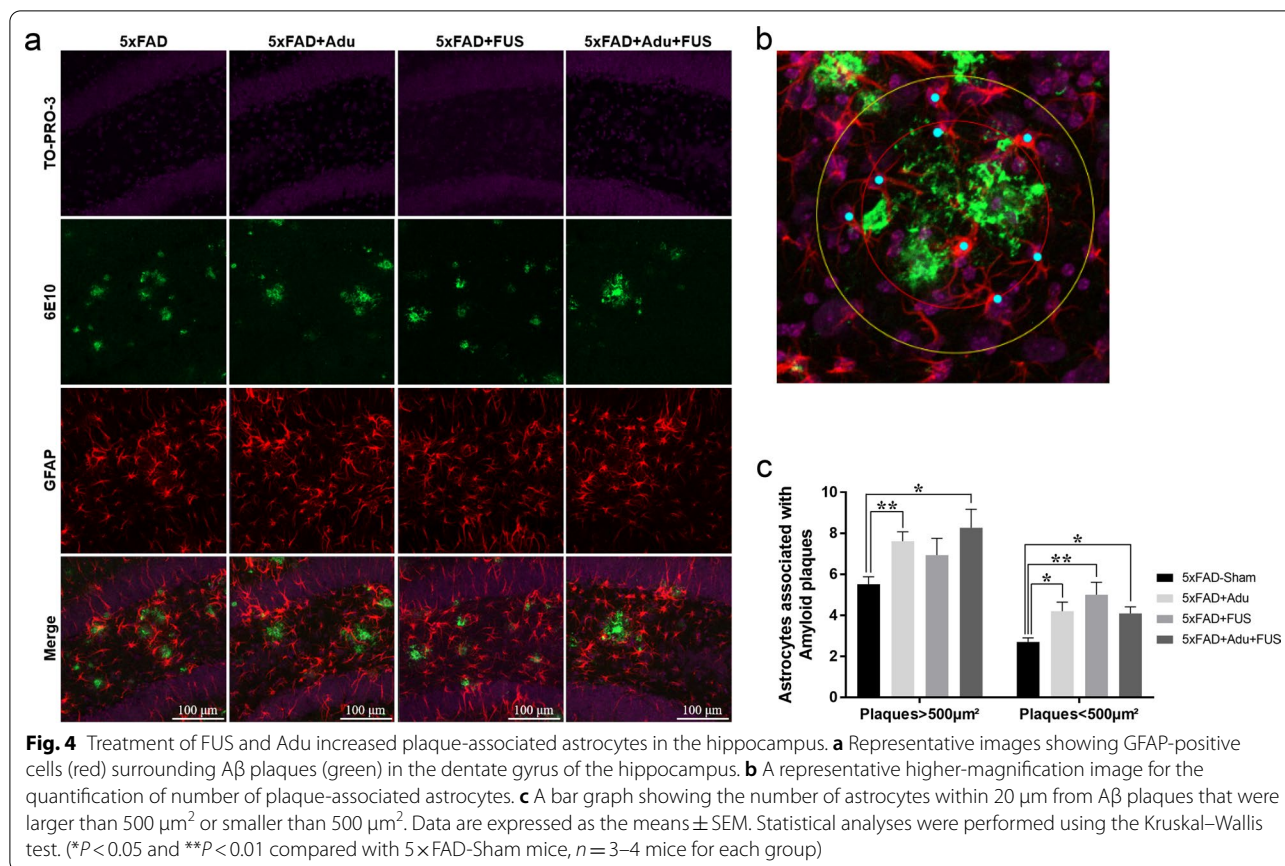
in the combined treatment group (Fig. 3e, 5x FAD-Sham: $26.6 \pm 4.7 \mu\text{m}^2$, 5x FAD + Adu: $27.5 \pm 10.1 \mu\text{m}^2$, 5x FAD + FUS: $33.0 \pm 6.6 \mu\text{m}^2$, and 5x FAD + FUS + Adu: $48.4 \pm 7.3 \mu\text{m}^2$).

Reactive astrocytes cluster around amyloid plaques, and the brain area occupied by these reactive astrocytes shows a significant increase in AD patients [30]. In addition, there are several lines of evidence that astrocytes can also eliminate amyloid plaques and neurons containing Aβ and enhance phagocytosis by microglia [31–33]. To investigate the number of amyloid plaque-associated astrocytes, we assessed the number of astrocytes within 20 μm from amyloid plaques. As shown in Fig. 4a, confocal images showed that reactive astrocytes were recruited to amyloid plaques in all groups. To describe how the number of astrocytes associated with plaques was measured, a higher-magnification image is shown in Fig. 4b. The recruitment of astrocytes surrounding amyloid plaques smaller than 500 μm² was enhanced in the 5x FAD + Adu group, the 5x FAD + FUS group, and the combined treatment group (Fig. 4c, 5x FAD-Sham: 2.7 ± 0.2 , 5x FAD + Adu: 4.20 ± 0.4 , 5x FAD + FUS: 5.0 ± 0.6 , 5x FAD + FUS + Adu: 4.1 ± 0.3 /amyloid plaque). The recruitment of astrocytes was increased in 5x FAD mice treated with Adu alone and the combination treatment surrounding amyloid plaques larger than 500 μm² (Fig. 4c, 5x FAD-Sham: 5.5 ± 0.3 , 5x FAD + Adu: 7.6 ± 0.4 , 5x FAD + FUS: 6.9 ± 0.8 , and

5x FAD + FUS + Adu: 8.2 ± 0.9 /amyloid plaques). These results suggest that the activation of microglia and the number of astrocytes associated with amyloid plaques were increased by the combined treatment with FUS and Adu.

Combined treatment with FUS and Adu increased neurogenesis in the hippocampi of 5x FAD mice

Adult hippocampal neurogenesis is normally active in neurologically normal subjects and decreases severely in patients with AD [34]. To determine whether repeated treatment affects the survival of labeled cells in the hippocampus, half of each group was injected with BrdU after the 1st treatment. The rest of mice was injected after the 3rd treatment to measure the cell proliferation and differentiation activity following the 3rd treatment. We quantified the cells stained with BrdU which is incorporated into dividing cells during the S-phase of the cell cycle and is a marker of newborn cells [35], and NeuN, a neuronal marker in the subgranular zone and granular cell layer of the dentate gyrus (Fig. 5a). The numbers of BrdU⁺ and BrdU⁺/NeuN⁺ cells after the 1st treatment and after the 3rd treatment were compared. Only the combined treatment group (6.5 ± 0.8) showed a significantly increased number of BrdU⁺ cells in the hippocampus, compared with the 5x FAD-Sham group (3.1 ± 0.8) after the 1st and 3rd treatments (Fig. 5b and

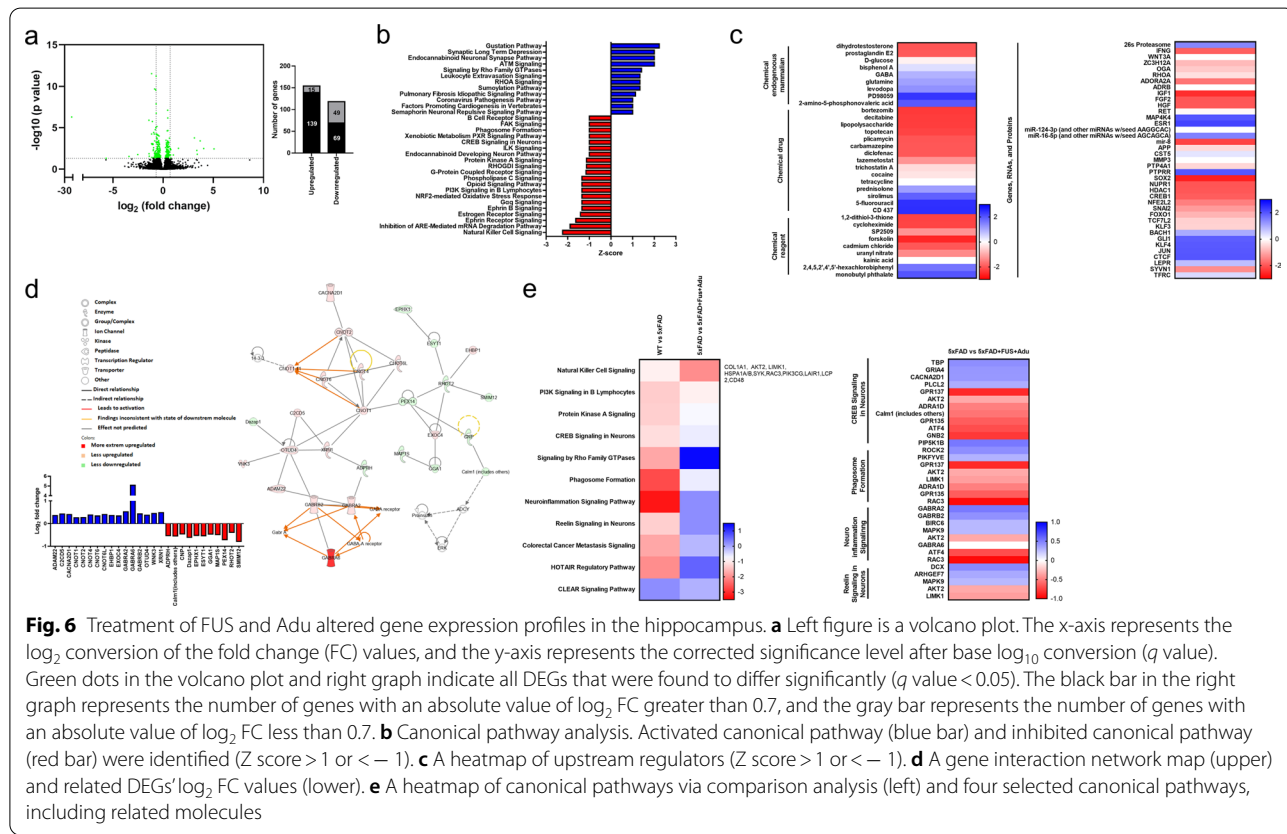
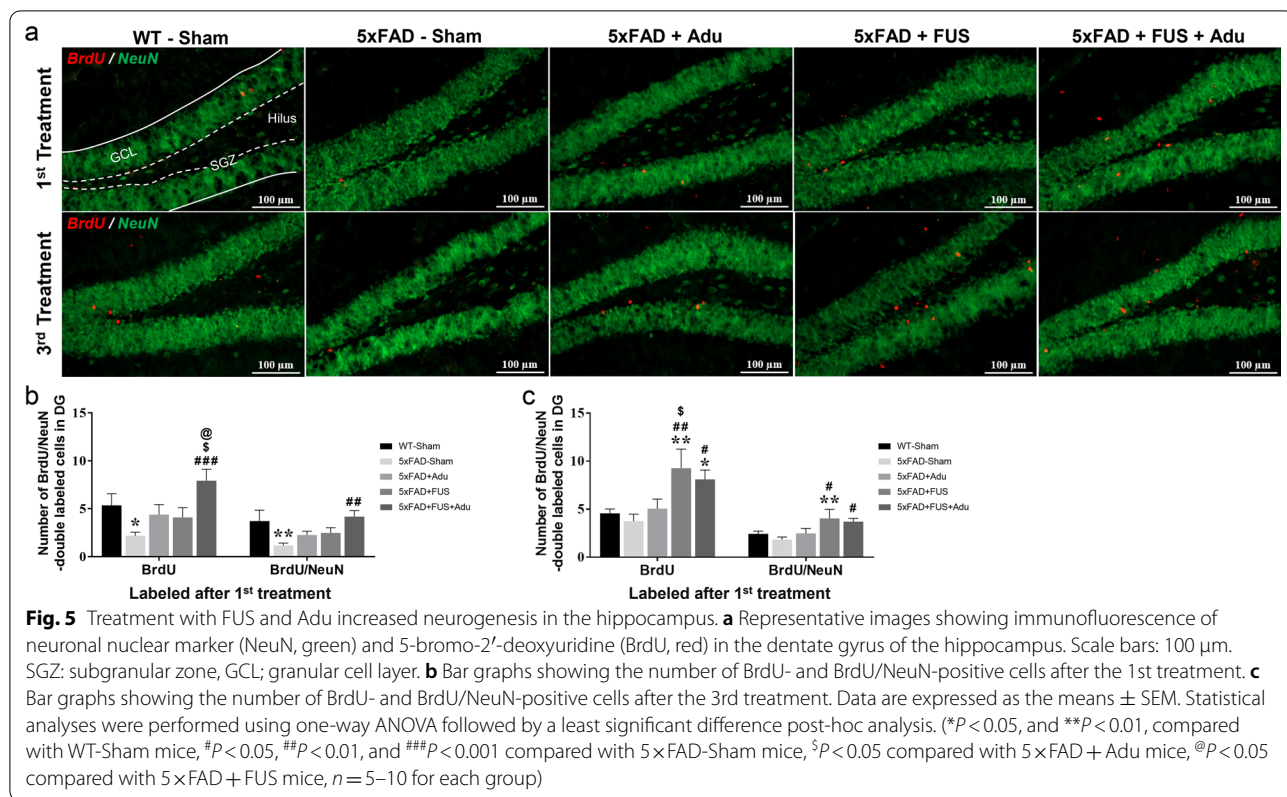


c). The combined treatment group (3.5 ± 0.5) also exhibited a highly increased number of BrdU⁺/NeuN⁺ cells compared with 5 × FAD-Sham (1.6 ± 0.2) after the 1st and 3rd treatments (Fig. 5b and c). Interestingly, when BrdU was injected after the 3rd treatment, the proliferation rate was significantly higher in the FUS alone group than in the combined treatment group. Overall, these results indicate that the combined treatment of FUS and Adu increases proliferation and survival of differentiated neural cells and induces remarkable neurogenesis in the hippocampus.

DEGs associated with inflammation and synaptic plasticity pathways were revealed via transcriptome profiling in the hippocampi of 5 × FAD mice treated with FUS and Adu

To understand the underlying action mechanisms related to the recovery of cognitive impairments and neuropathological characteristics by treatment with FUS combined with Adu in 5 × FAD mice, RNA sequencing was performed in the hippocampi of the experimental animal groups. As shown Fig. 6a, a total of 21,833 DEGs were identified and displayed as a volcano plot. Among these genes, 146 DEGs were up-regulated and 128 DEGs were

down-regulated significantly ($q < 0.05$). Among the 274 annotated DEGs, a functional prediction analysis was performed using IPA software (Fig. 6b–e). For canonical pathway analysis, a total of 32 enriched canonical pathways were identified by applying absolute *z* scores greater than 1. Among these pathways, a total of 12 pathways and 20 pathways were activated and inhibited, respectively (Fig. 6b). Furthermore, a total of 276 upstream regulators which modulate DEGs were identified by applying the *p* value of overlap < 0.05 threshold. Among them, 30 molecules were predicted to be activated and 43 molecules were predicted to be inhibited (Fig. 6c). We also analyzed the network to show the interactions between molecules in the dataset (Fig. 6d). The highest ranked network which was sorted using the score values (score 49), was found to mainly affect ‘neurological disease, psychological disorder, organismal injury and abnormalities’, involving 27 molecules. We found that 16 DEGs (*ADAM22*, *C2CD5*, *CACNA2D1*, *CNOT1*, *CNOT2*, *CNOT4*, *CNOT6*, *CNOT6L*, *EHBPI*, *EXOC4*, *GABRA2*, *GABRA6*, *GABRB2*, *OTUD4*, *WNK3* and *RN1*) were up-regulated and 11 DEGs (*ADPRH*, *Calm1*, *CNP*, *Dazap1*, *EPHX1*, *ESYT1*, *GGA1*, *MAP1S*, *PEX14*, *RHOT2*, and *SMIM12*) were down-regulated in the network. To



investigate the similarity, difference and trend between the WT-Sham and 5×FAD-Sham and between 5×FAD-Sham and 5×FAD + FUS + Adu datasets, a comparison analysis was performed using the comparison analysis function in IPA. As shown Fig. 6e, a total of 11 canonical pathways were found to be enriched in comparison analysis. In particular, four canonical pathways (phagosome formation, neuroinflammation signaling, CREB signaling in neurons and reelin signaling in neurons) were ameliorated in 5×FAD + FUS + Adu mice compared with 5×FAD mice. Taken together, our data revealed that combined treatment with FUS and Adu altered pathways in the hippocampus that are related to neuroinflammation and neural activity.

Discussion

The BBB hinders therapeutic agents from penetrating into the brain and becomes an obstacle to CNS disease treatment [36]. Previously, we reported several studies regarding BBB opening by FUS [20, 27]. The safety of FUS has already been verified, and it has been currently used in clinical trials [11, 37, 38].

A significant correlation between cognitive decline and brain amyloid plaque levels in the living brain evaluated using PET-CT scan has been reported [39]. Recently, the FDA approved Adu for the treatment of AD based on an evaluation of effects of the drug in clinical stages [5, 40]. However, the high dose of Adu (10–60 mg/kg) used in clinical studies induced ARIA-E in human clinical phases [41]. According to the study, patients who were treated with 10 mg/kg of Adu experienced ARIA-E with headache, confusion, dizziness and nausea; microhemorrhage; and superficial siderosis in clinical phase 3. Therefore, delivering an appropriate dose of Adu may be a key point for safety and effectiveness in AD.

In this study, we aimed to investigate whether the combined treatment with FUS and Adu improves the very low BBB penetration ratio of Adu caused by its large molecular weight (approximately 150 kDa) in systemic administration. We first confirmed that FUS safely opened the BBB (Fig. 1c). The Western blotting and immunofluorescence results demonstrated that the delivery of Adu was improved by FUS-mediated BBB opening (Fig. 1d–f, Additional file 1: Fig. S2). Additionally, FUS induced localized BBB opening and the opening was closed within 24 h (data not shown). These data imply that FUS is a potential and safe method to reversibly enhance BBB permeability and improve cerebral drug delivery.

Here, the impairments in cognitive function and the accumulation of amyloid plaques were ameliorated at a low dose of Adu (3 mg/kg) with FUS in 5×FAD mice (Fig. 2). While the combined treatment group only showed significant restoration of cognitive impairment,

spontaneous alternation Y-maze test did not show any significant difference between the FUS alone or Adu alone group and 5×FAD-Sham group. Notably, the combined treatment resulted in a marked improvement in cognitive impairment after the 3rd treatment (Fig. 2c). In addition, we also examined neuropathological changes, especially the amyloid plaque levels in the hippocampus, after treatment in 5×FAD mice. The number of amyloid plaques was decreased in the hippocampi of the 5×FAD + Adu, 5×FAD + FUS, and 5×FAD + FUS + Adu mice. In addition, the total area of the amyloid plaques was reduced in the hippocampi of the 5×FAD + FUS and 5×FAD + FUS + Adu mice (Fig. 2d–f). A previous report by others focused on the effects of a scanning ultrasound on the delivery of Adu into the brain and demonstrated that in APP23 mice, both the Adu only and scanning ultrasound only groups reduced the total plaque area in the hippocampus with no additive effect observed with the combination treatment of scanning ultrasound and Adu [15, 17, 42].

In our study, somewhat different aspects of FUS was investigated. Although the effects of FUS on BBB opening and on neurogenesis may have different mechanisms and different biological relevance to AD treatment, we expect their effects would be synergistic.

Even though the FDA approved the use of Adu via an accelerated approval program, the action mechanism underlying the treatment effects of Adu in the brain is still poorly understood. To understand the underlying mechanisms of action, we investigated the changes in microglia, astrocytes, and neurons after treatment with Adu in 5×FAD mice. Microglia are the only immune cells resident in the CNS, constitute 5%–10% of total brain cells, and take up, phagocytose, and proteolyse both soluble and fibrillar forms of A β [43, 44]. Phagocytes such as microglia express Fc receptors (FcRs) on the cell surface and bind to the Fc region of antibodies. FcR activates phagocytosis, clearance of myelin debris and the inflammatory response [45, 46]. The Fc portion of Adu can bind to FcRs expressed in microglia and opsonize A β for phagocytosis by microglia [47]. Early reports found that microglia surround amyloid plaques in the brains of AD patients, and A β fibrils were found within the microglia [48]. In this study, treatment with Adu alone increased the recruitment of microglia to amyloid plaques. This might induce a decrease in the number of amyloid plaques as shown in Fig. 2d and e. However, the combined treatment did not affect the number of microglia surrounding the amyloid plaques (Fig. 3c). This finding indicates that the recruitment of microglia around the amyloid plaques was not changed. Interestingly, a quantitative assessment of the CD68⁺/Iba-1⁺ area revealed a significant increase in the 5×FAD + FUS + Adu group

(Fig. 3e). Furthermore, we identified that the phagosome formation pathway (*PIP5K1B*, *ROCK2*, *PIKFYVE*, *GPR137*, *AKT2*, *LIMK1*, *ADRA1D*, *GPR135*, and *RAC3*) was activated in the combined treatment group using RNA sequencing and IPA (Fig. 6e). The activation of astrocytes, as demonstrated by increased GFAP expression, and amyloid deposition surrounded by activated astrocytes have a substantial impact on the AD state [49]. In the brains of AD patients and mouse models, there is a significant increase in GFAP immunoreactivities in plaque-associated astrocytes. Similar to the activation of microglia, reactive astrocytes phagocytose amyloid aggregates and dystrophic neurites and are involved in the inflammatory response to A β [33, 50]. Additionally, knockout of GFAP in an AD mouse model showed a twofold increase in amyloid plaque burden and twice the amounts of dystrophic neurites [51]. Astrocytes were reported to be activated and uptake more A β in the brains of MRI-guided FUS-treated mice [16]. Consistent with these results, we observed an increased number of plaque-associated astrocytes and a reduced number and size of amyloid plaques in hippocampi of the 5 \times FAD + Adu, 5 \times FAD + FUS, and 5 \times FAD + FUS + Adu mice (Figs. 2 and 4). Although treatment with Adu alone or FUS alone increased plaque-associated astrocytes, these increases were not sufficient to alleviate cognitive decline in the 5 \times FAD mice. Collectively, our data suggest that the combined treatment with FUS and Adu promotes glial phagocytosis (microglia and astrocytes) and clearance of A β , which may induce a reduction in A β deposition in the brains of the 5 \times FAD mice. To elucidate the precise molecular mechanisms of phagocytosis associated with these pathways, more in-depth study is required in both in vitro and in vivo models.

The neurotoxicity of amyloidogenic proteins was demonstrated to affect long-term potentiation, plasticity, synaptic signaling, dendritic morphology, and cognition in a preclinical study. This toxic microenvironment decreases the survival and proliferation of newborn cells in the hippocampus [52–54]. Our results showed that the combined treatment decreased amyloid plaque formation as shown in Fig. 2.

Previous studies have reported that FUS-mediated BBB opening induces hippocampal neurogenesis [17, 18]. In this study, we investigated whether the combined treatment also induces neurogenesis and compared the effects of the combined treatment with FUS or Adu alone. The three administrations of combined treatment with FUS and Adu led to increased survival of newly proliferating and differentiated neuronal cells compared with FUS or Adu alone. Indeed, BrdU-labeled cells after the last combined treatment and FUS alone showed increased proliferation and neuronal differentiation (Fig. 5).

Hippocampal neurogenesis plays a key role in long-term memory and cognitive function [55, 56]. Future research is needed to elucidate the difference between the results of the 1st and 3rd treatments. As neurogenesis is induced only when the BBB is opened, it is assumed that changes in the intravascular microenvironment or the components of the tight junction may have played a role in promoting neurogenesis. In addition, brain-derived neurotrophic factor (BDNF) is reported to be one of the most important factors in inducing neurogenesis, and there is a report that the FUS-mediated BBB opening increases the expression level of BDNF [20, 57]. Taken together, these results show that combined treatment enhances the survival of newborn cells, suggesting that Adu may potentially affect a part of the toxic microenvironment.

To understand the dynamic molecular processes induced by the combined treatment at the transcriptional level, transcriptome profiling was performed using RNA sequencing. We identified 32 canonical pathways based on significant DEGs that were submitted to IPA core analysis (Fig. 6a and b). To narrow the signaling pathways, a comparison analysis was conducted among multiple groups (WT vs 5 \times FAD and 5 \times FAD vs 5 \times FAD + FUS + Adu, Fig. 6e). We found four promising target canonical pathways, the neuroinflammation, phagosome formation, CREB and reelin signaling pathways. The combined treatment with FUS and Adu ameliorated neuroinflammation signaling which involved *GABRA2*, *GABRB2*, *BIRC6*, *MAPK9*, *AKT2*, *GABRA6*, *ATF4*, and *RAC3* and phagosome formation. These results may explain why microglia and astrocytes were activated by the combined treatment and may indicate which molecules are associated with neuroinflammation and phagocytosis (Figs. 3 and 4). Both CREB signaling (*TBP*, *GRIA4*, *CACNA2D1*, *PLCL2*, *GPR137*, *AKT2*, *ADRA1D*, *Calm1*, *GPR135*, *ATF4*, and *GNB2*) and reelin signaling (*DCX*, *ARHGEF7*, *MAPK9*, *AKT2*, and *LIMK1*) genes in neurons were proposed to be activated genes after combined treatment with FUS and Adu in 5 \times FAD (Fig. 6e). CREB signaling modulates synaptic plasticity by mediating the conversion of short- and long-term memory and has been involved in cognitive function [58]. Reelin signaling is also important in synaptic function, learning, and memory [59]. Thus, the comparison analysis supports the idea that cognitive impairment may be attenuated via these two pathways after combined treatment with FUS and Adu. Overall, transcriptome profiling suggests that gene sets related to an activated immune response (neuroinflammation and phagosome formation) in the brain and the inhibition of neuronal activity (CREB and reelin signaling) were reversed after combined treatment. Moreover, the IPA-derived gene network which provides direct and indirect relationships

among DEGs and DEG regulators, suggests that the categories of neurological disease, psychological disorders, organismal injury, and abnormalities were scored highly after combined treatment with FUS and Adu. In particular, GABAergic pathway-associated genes (*GABRB2*, *GABRA2* and *GABRA6*) involved in this category were predicted in 5×FAD + FUS + Adu mice through network analysis (Fig. 6d). Several studies have reported the role of impaired function of GABA_A receptors by modulating neuronal activity in AD [50, 51]. Accordingly, these results may indicate that the GABAergic pathway also plays a role after combined treatment with FUS and Adu. To investigate the specific biological progress of Adu therapy in AD, further in-depth studies are needed to validate the potential key molecules or mechanisms identified in the current study.

Conclusion

In conclusion, an effective treatment approach for AD is by improving cognitive function and reducing deposited amyloid plaques rather than alleviating symptoms and delaying progression. In this study, the enhanced delivery of a low dose of Adu (3 mg/kg) via FUS reduced amyloid deposits and restored spatial memory. In addition, it was proven to be effective in neuropathological changes such as enhanced phagocytosis and neurogenesis. Overall, this study provides insight into establishing a therapeutic strategy for the treatment of AD as well as other neurodegenerative diseases (Additional file 1: Fig. S4).

In this work, we demonstrated that FUS with microbubbles induced BBB opening and increased the delivery of Adu into the brain. In in vivo experiment, the combined treatment alleviated the pathology and improved cognitive function through glial stimulation and prevention of Aβ aggregation in the AD mouse model. In addition to achieving higher efficacy in the delivery and therapy, the combined treatment also showed safety in mice. This study suggests that the optimized delivery technology using FUS can be applied to other drugs for CNS diseases.

Abbreviations

Aβ: Amyloid-β; AD: Alzheimer's disease; Adu: Aducanumab; ARIA-E: Abnormalities including edema; BBB: Blood–brain barrier; BDNF: Brain-derived neurotrophic factor; BrdU: 5-Bromo-2'-deoxyuridine; CNS: Central nervous system; DEG: Differentially expressed gene; FcR: Fc receptor; FUS: Focused ultrasound; GABA: Gamma-aminobutyric acid; GCL: Granular cell layer; GFAP: Glial fibrillary acidic protein; IPA: Ingenuity pathway analysis; MRI: Magnetic resonance imaging; NeuN: Neuronal nuclei; PBS: Phosphate-buffered saline; RNA: Ribonucleic acid; ROI: Region of interest; SGZ: Subgranular zone; WT: Wild type.

Supplementary Information

The online version contains supplementary material available at <https://doi.org/10.1186/s40035-022-00333-x>.

Additional file 1. Fig. S1: The protein level of ZO-1 in 6-month-old WT-Sham, 5×FAD-Sham, 5×FAD+Adu, 5×FAD+FUS and 5×FAD+FUS+Adu mice. A representative blot of ZO-1 in the hippocampus is shown. **Fig. S2:** Brain delivery of Adu by FUS occurred in a dose-dependent manner and was examined 24 hours after FUS sonication in 6-month-old 5×FAD mice. A representative blot of Adu assessed with human IgG in the hippocampus is shown. **Fig. S3:** The Adu concentration in mouse serum after Adu treatment at two time points, 1 hour (white) and 24 hours (gray). A bar graph showing the levels of Adu determined using anti-human IgG antibody in serum. Data are presented as mean ± SEM. Statistical analyses were performed using one-way ANOVA, followed by Tukey's post-hoc test. (**P* < 0.05, ***P* < 0.01 compared with 5×FAD+Adu mice, *n* = 3 for each group). **Fig. S4:** Summary figure. Schematic diagram of the combined therapy of FUS and Adu. FUS can be used in conjunction with microbubbles to temporarily open the BBB, thereby allowing delivery of Adu into the brain. Due to the combined effect of FUS and Adu, neurogenesis and phagocytosis are increased and amyloid plaques are decreased.

Acknowledgements

We would like to thank professor Young Cheol Na for comments. And also, we thank the Bioinformatics Collaboration Unit, Yonsei University College of Medicine for the RNA sequencing analysis support.

Author contributions

JWC, H-SK, and HK conceptualized the project. CK, E-JY, JWS, C-HL, JP, S-HK, S-WP and WSC performed the experiments and analyzed the data. HK and CK prepared the manuscript with contributions from all authors. All authors read and approved the final manuscript.

Funding

This study was financially supported by grants from the Healthcare Technology R&D Project (HI19C0060) by the Ministry for Health, Welfare, and Family Affairs, Republic of Korea. In addition, this work was supported by Seoul National University Bundang Hospital Research Fund, South Korea (14–2021-0004) and National Research Foundation of Korea (NRF) grant funded by the Korea government (MIST) (Grant no. 2020R1A2C1011839) to HS. Kim. Also, H. Kim and E.J. Yang received a scholarship from the BK21-Plus Education Program provided by the National Research Foundation of Korea.

Availability of data and materials

The datasets used and/or analyzed in the current study are available from the corresponding authors on reasonable request.

Declarations

Ethics approval and consent to participate

All works involving animals were approved by the Institute for Experimental Animals of Seoul National University. Also, all experiments were approved by the Animal Care Committee of Seoul National University (Approval Number: SNU-201005-2-1).

Consent for publication

All the authors have approved the manuscript.

Competing interests

The authors declare that they have no competing interests.

Author details

¹Department of Neurosurgery, Yonsei University College of Medicine, 50 Yonsei-Ro, Seodaemun-Gu, Seoul, Republic of Korea. ²Department of Pharmacology, College of Medicine, Seoul National University, 103 Daehakro, Jongro-Gu, Seoul, Republic of Korea. ³Neuroscience Research Center, College of Medicine, Seoul National University, 103 Daehakro, Jongro-Gu, Seoul, Republic of Korea. ⁴Department of Biomedical Sciences, College of Medicine, Seoul National University, 103 Daehakro, Jongro-Gu, Seoul, Republic of Korea. ⁵Bundang Hospital, Seoul National University College of Medicine, Bundang-Gu, Sungnam, Republic of Korea.

Received: 26 July 2022 Accepted: 8 December 2022
Published online: 27 December 2022

References

- Tampi RR, Forester BP, Agronin M. Aducanumab: evidence from clinical trial data and controversies. *Drugs Context*. 2021. <https://doi.org/10.7573/dic.2021-7-3>.
- Cummings J, Lee G, Ritter A, Sabbagh M, Zhong K. Alzheimer's disease drug development pipeline: 2020. *Alzheimer's Dement Transl Res Clin Interv*. 2020;6(1):e12050.
- Cummings J, Lee G, Zhong K, Fonseca J, Taghva K. Alzheimer's disease drug development pipeline: 2021. *Alzheimer's Dement Transl Res Clin Interv*. 2021;7(1):e12179.
- Dunn B, Stein P, Cavazzoni P. Approval of aducanumab for Alzheimer disease—the FDA's perspective. *JAMA Intern Med*. 2021;181(10):1276–8.
- Sevigny J, Chiao P, Bussi ere T, Weinreb PH, Williams L, Maier M, et al. The antibody aducanumab reduces A β plaques in Alzheimer's disease. *Nature*. 2016;537(7618):50–6.
- Pardridge WM. The blood-brain barrier: bottleneck in brain drug development. *NeuroRx*. 2005;2(1):3–14.
- Hynynen K, McDannold N, Sheikov NA, Jolesz FA, Vykhodtseva N. Local and reversible blood–brain barrier disruption by noninvasive focused ultrasound at frequencies suitable for trans-skull sonications. *Neuroimage*. 2005;24(1):12–20.
- Hynynen K, McDannold N, Vykhodtseva N, Jolesz FA. Noninvasive MR imaging-guided focal opening of the blood-brain barrier in rabbits. *Radiology*. 2001;220(3):640–6.
- Treat LH, McDannold N, Zhang Y, Vykhodtseva N, Hynynen K. Improved anti-tumor effect of liposomal doxorubicin after targeted blood-brain barrier disruption by MRI-guided focused ultrasound in rat glioma. *Ultrasound Med Biol*. 2012;38(10):1716–25.
- Alli S, Figueiredo CA, Golbourn B, Sabha N, Wu MY, Bondoc A, et al. Brainstem blood brain barrier disruption using focused ultrasound: a demonstration of feasibility and enhanced doxorubicin delivery. *J Control Release*. 2018;281:29–41.
- Park SH, Kim MJ, Jung HH, Chang WS, Choi HS, Rachmilevitch I, et al. One-year outcome of multiple blood–brain barrier disruptions with temozolomide for the treatment of glioblastoma. *Front Oncol*. 2020;10:1663.
- Alkins R, Burgess A, Kerbel R, Wels WS, Hynynen K. Early treatment of HER2-amplified brain tumors with targeted NK-92 cells and focused ultrasound improves survival. *Neuro Oncol*. 2016;18(7):974–81.
- Burgess A, Ayala-Grosso CA, Ganguly M, Jord ao JF, Aubert I, Hynynen K. Targeted delivery of neural stem cells to the brain using MRI-guided focused ultrasound to disrupt the blood-brain barrier. *PLoS ONE*. 2011;6(11):e27877.
- Lee J, Chang WS, Shin J, Seo Y, Kong C, Song B-W, et al. Non-invasively enhanced intracranial transplantation of mesenchymal stem cells using focused ultrasound mediated by overexpression of cell-adhesion molecules. *Stem Cell Res*. 2020;43:101726.
- Leinenga G, G otz J. Scanning ultrasound removes amyloid- β and restores memory in an Alzheimer's disease mouse model. *Sci Transl Med*. 2015;7(278):278.
- Jord ao JF, Th evenot E, Markham-Coultes K, Scarcelli T, Weng YQ, Xhima K, et al. Amyloid- β plaque reduction, endogenous antibody delivery and glial activation by brain-targeted, transcranial focused ultrasound. *Exp Neurol*. 2013;248:16–29.
- Leinenga G, G otz J. Safety and efficacy of scanning ultrasound treatment of aged APP23 mice. *Front Neurosci*. 2018;12:55.
- Scarcelli T, Jord ao JF, O'Reilly MA, Ellens N, Hynynen K, Aubert I. Stimulation of hippocampal neurogenesis by transcranial focused ultrasound and microbubbles in adult mice. *Brain Stimul*. 2014;7(2):304–7.
- Mooney SJ, Shah K, Yeung S, Burgess A, Aubert I, Hynynen K. Focused ultrasound-induced neurogenesis requires an increase in blood-brain barrier permeability. *PLoS ONE*. 2016;11(7):e0159892.
- Shin J, Kong C, Lee J, Choi BY, Sim J, Koh CS, et al. Focused ultrasound-induced blood-brain barrier opening improves adult hippocampal neurogenesis and cognitive function in a cholinergic degeneration dementia rat model. *Alzheimer's Res Ther*. 2019;11(1):1–15.
- Oakley H, Cole SL, Logan S, Maus E, Shao P, Craft J, et al. Intraneuronal β -amyloid aggregates, neurodegeneration, and neuron loss in transgenic mice with five familial Alzheimer's disease mutations: potential factors in amyloid plaque formation. *J Neurosci*. 2006;26(40):10129–40.
- Devi L, Ohno M. Phospho-eIF2 α level is important for determining abilities of BACE1 reduction to rescue cholinergic neurodegeneration and memory defects in 5 \times FAD mice. *PLoS ONE*. 2010;5(9):e12974.
- Eimer WA, Vassar R. Neuron loss in the 5 \times FAD mouse model of Alzheimer's disease correlates with intraneuronal A β 42 accumulation and Caspase-3 activation. *Mol Neurodegener*. 2013;8(1):1–12.
- Stine WB, Jungbauer L, Yu C, LaDu MJ. Preparing synthetic A β in different aggregation states. In: *Alzheimer's Disease and Frontotemporal Dementia*: Springer; 2010. p. 13–32.
- Lee S, Varvel NH, Konerth ME, Xu G, Cardona AE, Ransohoff RM, et al. CX3CR1 deficiency alters microglial activation and reduces beta-amyloid deposition in two Alzheimer's disease mouse models. *Am J Pathol*. 2010;177(5):2549–62.
- Sheikov N, McDannold N, Sharma S, Hynynen K. Effect of focused ultrasound applied with an ultrasound contrast agent on the tight junctional integrity of the brain microvascular endothelium. *Ultrasound Med Biol*. 2008;34(7):1093–104.
- Shin J, Kong C, Cho JS, Lee J, Koh CS, Yoon MS, et al. Focused ultrasound-mediated noninvasive blood-brain barrier modulation: preclinical examination of efficacy and safety in various sonication parameters. *Neurosurg Focus*. 2018;44(2):E15.
- Ries M, Sastre M. Mechanisms of A β clearance and degradation by glial cells. *Front Aging Neurosci*. 2016;8:160.
- Hopperton K, Mohammad D, Tr epanier M, Giuliano V, Bazinet R. Markers of microglia in post-mortem brain samples from patients with Alzheimer's disease: a systematic review. *Mol Psychiatry*. 2018;23(2):177–98.
- Perez-Nievas BG, Serrano-Pozo A. Deciphering the astrocyte reaction in Alzheimer's disease. *Front Aging Neurosci*. 2018;10:114.
- Koistinaho M, Lin S, Wu X, Esterman M, Koger D, Hanson J, et al. Apolipoprotein E promotes astrocyte colocalization and degradation of deposited amyloid- β peptides. *Nat Med*. 2004;10(7):719–26.
- Lian H, Litvinchuk A, Chiang AC-A, Aithmitti N, Jankowsky JL, Zheng H. Astrocyte-microglia cross talk through complement activation modulates amyloid pathology in mouse models of Alzheimer's disease. *J Neurosci*. 2016;36(2):577–89.
- Nagele RG, D'Andrea MR, Lee H, Venkataraman V, Wang H-Y. Astrocytes accumulate A β 42 and give rise to astrocytic amyloid plaques in Alzheimer disease brains. *Brain Res*. 2003;971(2):197–209.
- Moreno-Jim enez EP, Flor-Garc ia M, Terreros-Roncal J, R abano A, Cafini F, Pallas-Bazarra N, et al. Adult hippocampal neurogenesis is abundant in neurologically healthy subjects and drops sharply in patients with Alzheimer's disease. *Nat Med*. 2019;25(4):554–60.
- Taupin P. BrdU immunohistochemistry for studying adult neurogenesis: paradigms, pitfalls, limitations, and validation. *Brain Res Rev*. 2007;53(1):198–214.
- Luo K, Wang Y, Chen W-S, Feng X, Liao Y, Chen S, et al. Treatment combining focused ultrasound with gastrodin alleviates memory deficit and neuropathology in an Alzheimer's disease-like experimental mouse model. *Neural plasticity*. 2022;2022.
- Meng Y, Reilly RM, Pezo RC, Trudeau M, Sahgal A, Singnurkar A, et al. MR-guided focused ultrasound enhances delivery of trastuzumab to HER2-positive brain metastases. *Sci Transl Med*. 2021;13(615):eabj4011.
- Lipsman N, Meng Y, Bethune AJ, Huang Y, Lam B, Masellis M, et al. Blood-brain barrier opening in Alzheimer's disease using MR-guided focused ultrasound. *Nat Commun*. 2018;9(1):1–8.
- Braskie MN, Thompson PM. Understanding cognitive deficits in Alzheimer's disease based on neuroimaging findings. *Trends Cogn Sci*. 2013;17(10):510–6.
- Swanson CJ, Zhang Y, Dhadda S, Wang J, Kaplow J, Lai RY, et al. A randomized, double-blind, phase 2b proof-of-concept clinical trial in early Alzheimer's disease with lecanemab, an anti-A β protofibril antibody. *Alzheimer's Res Ther*. 2021;13(1):1–14.
- Salloway S, Chalkias S, Barkhof F, Burkett P, Barakos J, Purcell D, et al. Amyloid-related imaging abnormalities in 2 phase 3 studies evaluating aducanumab in patients with early Alzheimer disease. *JAMA Neurol*. 2022;79(1):13–21.

42. Leinenga G, Koh WK, Götz J. A comparative study of the effects of Aducanumab and scanning ultrasound on amyloid plaques and behavior in the APP23 mouse model of Alzheimer disease. *Alzheimer's Res Ther.* 2021;13(1):1–14.
43. Reed-Geaghan EG, Savage JC, Hise AG, Landreth GE. CD14 and toll-like receptors 2 and 4 are required for fibrillar A β -stimulated microglial activation. *J Neurosci.* 2009;29(38):11982–92.
44. Tahara K, Kim HD, Jin JJ, Maxwell JA, Li L, Fukuchi KI. Role of toll-like receptor signalling in A β uptake and clearance. *Brain.* 2006;129(11):3006–19.
45. Kang SH, Lee C-H. Development of therapeutic antibodies and modulating the characteristics of therapeutic antibodies to maximize the therapeutic efficacy. *Biotechnol Bioprocess Eng.* 2021;26(3):295–311.
46. Lee C-H, Kang TH, Godon O, Watanabe M, Delidakis G, Gillis CM, et al. An engineered human Fc domain that behaves like a pH-toggle switch for ultra-long circulation persistence. *Nat Commun.* 2019;10(1):1–11.
47. Crehan H, Liu B, Kleinschmidt M, Rahfeld J-U, Le KX, Caldarone BJ, et al. Effector function of anti-pyroglutamate-3 A β antibodies affects cognitive benefit, glial activation and amyloid clearance in Alzheimer's-like mice. *Alzheimer's Res Ther.* 2020;12(1):1–19.
48. Perlmutter LS, Barron E, Chui HC. Morphologic association between microglia and senile plaque amyloid in Alzheimer's disease. *Neurosci Lett.* 1990;119(1):32–6.
49. Maragakis NJ, Rothstein JD. Mechanisms of disease: astrocytes in neurodegenerative disease. *Nat Clin Pract Neurol.* 2006;2(12):679–89.
50. Grathwohl SA, Kälin RE, Bolmont T, Prokop S, Winkelmann G, Kaeser SA, et al. Formation and maintenance of Alzheimer's disease β -amyloid plaques in the absence of microglia. *Nat Neurosci.* 2009;12(11):1361–3.
51. Kraft AW, Hu X, Yoon H, Yan P, Xiao Q, Wang Y, et al. Attenuating astrocyte activation accelerates plaque pathogenesis in APP/PS1 mice. *FASEB J.* 2013;27(1):187.
52. Shankar GM, Li S, Mehta TH, Garcia-Munoz A, Shepardson NE, Smith I, et al. Amyloid- β protein dimers isolated directly from Alzheimer's brains impair synaptic plasticity and memory. *Nat Med.* 2008;14(8):837–42.
53. Cleary JP, Walsh DM, Hofmeister JJ, Shankar GM, Kuskowski MA, Selkoe DJ, et al. Natural oligomers of the amyloid- β protein specifically disrupt cognitive function. *Nat Neurosci.* 2005;8(1):79–84.
54. Walsh DM, Klyubin I, Fadeeva JV, Cullen WK, Anwyl R, Wolfe MS, et al. Naturally secreted oligomers of amyloid β protein potently inhibit hippocampal long-term potentiation in vivo. *Nature.* 2002;416(6880):535–9.
55. Toda T, Gage FH. Adult neurogenesis contributes to hippocampal plasticity. *Cell Tissue Res.* 2018;373(3):693–709.
56. Lazarov O, Mattson MP, Peterson DA, Pimplikar SW, van Praag H. When neurogenesis encounters aging and disease. *Trends Neurosci.* 2010;33(12):569–79.
57. Rossi C, Angelucci A, Costantin L, Braschi C, Mazzantini M, Babbini F, et al. Brain-derived neurotrophic factor (BDNF) is required for the enhancement of hippocampal neurogenesis following environmental enrichment. *Eur J Neurosci.* 2006;24(7):1850–6.
58. Saura CA, Valero J. The role of CREB signaling in Alzheimer's disease and other cognitive disorders. *Rev Neurosci.* 2011;22(2):153–69.
59. Jossin Y. Reelin functions, mechanisms of action and signaling pathways during brain development and maturation. *Biomolecules.* 2020;10(6):964.

Ready to submit your research? Choose BMC and benefit from:

- fast, convenient online submission
- thorough peer review by experienced researchers in your field
- rapid publication on acceptance
- support for research data, including large and complex data types
- gold Open Access which fosters wider collaboration and increased citations
- maximum visibility for your research: over 100M website views per year

At BMC, research is always in progress.

Learn more biomedcentral.com/submissions

